Thermal Monitoring of Hydrothermal Activity by Permanent Infrared Automatic Stations. Results Obtained at Solfatara di Pozzuoli, Campi Flegrei (Italy)

Chiodini G., Vilardo G., Augusti V., Granieri D., Caliro S., Minopoli C., Terranova C.

Abstract

A permanent automatic infrared (IR) station was installed at Solfatara crater, the most active zone of Campi Flegrei caldera. After a positive in situ calibration of the IR camera, we analyze 2175 thermal IR images of the same scene from 2004 to 2007. The scene includes a portion of the steam heated hot soils of Solfatara. The experiment was initiated to detect and quantify temperature changes of the shallow thermal structure of a quiescent volcano such as Solfatara over long periods. Ambient temperature results as the main parameter affecting IR temperatures while air humidity and rain control image quality. A geometric correction of the images was necessary to remove the effects of slow movement of the camera. After a suitable correction the images give a reliable and detailed picture of the temperature changes, over the period October 2004 – January 2007, which suggests origin of the changes were linked to anthropogenic activity, vegetation growth and to the increase of the flux of hydrothermal fluids in the area of the hottest fumaroles. Two positive temperature anomalies were registered after the occurrence of two seismic swarms which affected the hydrothermal system of Solfatara in October 2005 and October 2006. It is worth noting that these signs were detected in a system characterized by a low level of activity with respect to systems affected by real volcanic crisis where more spectacular results will be expected. Results of the experiment show that this kind of monitoring system can be a suitable tool for volcanic surveillance.

1. Introduction

Quiescent volcanoes can release large amount of energy through the emission of hot fluids from diffuse degassing structures [*Werner et al.*, 2000; *Chiodini et al.*, 2001; *Ingebritsen et al.*, 2001; *Caliro et al.*, 2004; *Chiodini et al.*, 2005; *Hochstein and Bromley*, 2005; *Werner et al.*, 2006]. The process causes both soil diffuse degassing of incondensable hydrothermal gases, mainly CO_2, and the formation of hot soils because most of the original steam condenses at depth heating the ground. At Solfatara, located within the Campi Flegrei (CF) caldera, soil degassing of deeply derived CO_2 is spatially associated with hot soils over an area of about 0.5 km^2 (Fig. 1). The energy dissipated daily by the deeply heated soils represents the main flux of energy of the entire CF in the current period of quiescence. According to *Chiodini et al.* [2001] the thermal energy released from Solfatara by degassing (~ 100 MW) is much higher not only than the conductive heat flux over the caldera (90 km^2), but even than the average energy release associated to seismic activity and ground deformation in the last 30 years, a period during which two main uplift phases were recorded in 1969–1972 and in 1982–1984, respectively. In both cases, deformation was confined within a radius of 6 km, with maximum values of ~ 2 m at the caldera centre. There, the town of Pozzuoli was partially evacuated in 1984 due to the intense seismic activity [*Barberi et al.*, 1984]. Since 1985, a slow subsiding phase began and has been interrupted four times by minor uplifts in 1989, 1994, 2000, 2005-2006.

The pivotal role of the hydrothermal system in the genesis of the CF bradyseismic events was highlighted by recent interpretations of geophysical and geochemical signals [*Chiodini et al.*, 2003; *Todesco et al.*, 2004; *Todesco and Berrino*, 2005; *Battaglia et al.*, 2006; *Troise et al.*, 2007]. Nevertheless no data are available on the variations which affected the main flux of energy from the hydrothermal system of CF during this period of crisis, i.e. the thermal energy released at Solfatara. The monitoring of such energy fluxes may be a primary tool in the surveillance of volcanic activity at CF as well at other quiescent volcanoes of the world characterized by intense hydrothermal activity. With the aim of cover this gap in 2004 started the TIIMNet project (Thermal Infrared Imagery Monitoring Network) founded by the Italian National Operating Program for the realization of Infrared (IR) automatic stations specific for the monitoring of the shallow thermal structure of the hydrothermal zones of volcanoes. With respect to the traditional thermocouple measurements, which can be done only in selected sites, a single IR image can cover a large part of a fumarolic field resulting particularly useful for monitoring purposes. The IR images can in fact potentially register temperature variations occurring in any sector of the monitored scene. In addition the IR devices, which do not require a direct contact with the monitored target, result of easier maintenance with respect to the thermocouples often damaged by the high temperature and corrosive volcanic environment.

In recent years, IR based techniques have been largely used in applied volcanology. IR (0.9 - 13 µm) remote sensing of surface temperatures from space sensors has been applied to several volcanoes to monitor extent and magnitude of thermal activity associate with phenomena such as lava flows, active domes, fumaroles, hot springs, crater lakes or to detect and track eruption clouds [*Oppenheimer and Yirgu,* 2002; *Dean et al.,* 2004; *Harris et al.,* 2004; *Hellman and Ramsey,* 2004; *Watson et al.,* 2004; *Bailey et al.,* 2006]. In recent years, following the hand-held thermal imaging cameras development, increasing use is being made of ground-based thermal IR measurements to map and investigate lava flow field structures (flow field inflation, lava tube formation, vent migration, lava vesicularity), to estimate active lava flow parameters (e.g. effusion rate), to analyze the evolution of active eruption plumes [*Ramsey and Fink,* 1999; *Harris and Maciejewski,* 2000; *Pinkerton et al.,* 2002; *Calvari and Pinkerton,* 2004; *Lautze et al.,* 2004; *Calvari et al.,* 2005; *Johnson et al.,* 2005; *Harris et al.,* 2005; *Vaughan et al.,* 2005; *Lodato et al.,* 2006].

With respect to previous IR applications, most of which are focussed on the study of relatively quick processes associated to volcanic eruptions, our experiment has the aim to detect and quantify slow temperature changes of the shallow thermal structure of quiescent volcanoes over long periods. Any increase of fluid expelled by a volcano system will be accompanied by an increase in the temperature of the rocks hosting the fumarolic vents or in the size of the fumarolically heated areas [*Oppenheimer et al.,* 1993; *Kaneko and Wooster,* 1999]. Moreover, we think that also relatively slow variations in the amount of thermal energy flux can help to define the level of activity of the volcano and that possible major changes in surface temperature can mark the transition from a quiescent stage to an eruptive phase. For this reason our experiment was designed to monitor a significant portion of the Solfatara fumarolic field with a systematic periodic acquisition of IR images from a permanent station.

We present herein a comprehensive time series of night-time IR images for the 2004-2006, a period during which the station located at Solfatara acquired 2175 scenes. To our knowledge, this is the more comprehensive of such datasets available for a volcanic area.

In the first part of the paper we described the experiment design including the technical aspects of the IR camera and of the remote control system, the main characteristics of the monitored scene during the period October 2004-January 2007, and finally the in situ calibration test. In the second part of the paper the entire IR dataset is analyzed with the dual purpose to evaluate the thermal features of the Solfatara crater in the observation period and to determine whether IR information can be useful in the long period monitoring of a volcanically active area.

2. Experiment design

2.1 The remote control of the IR camera and the acquired scene

The IR camera used in the experiment is a NEC Thermo Tracer TS7302 that operates in the spectral range from 8 to 14 µm across a 29° (H) x 22° (V) field of view and a focusing range from 0.5 m to infinity with standard lens. It is a camera with uncooled focal plane array measuring systems (microbolometer technology 320x240 pixel) of recent availability for civil purposes.

Such a system has found extensive usage in permanent configurations for process and quality control in production line and the monitoring of systems in motion or electrical devices; therefore, such monitoring applications imply that thermal cameras are laboratory instruments or just predisposed for indoor installations.

Similar experiments of IR camera use have never been carried out for long period outdoor in extreme conditions as those affecting a volcanic area. For this reason, the first part of the experiment was devoted to integrate the station with protective housing and remote monitoring system (RMS) including data transmission devices. A picture of the Solfatara station is shown in Fig. 2a.

The camera was placed inside a protective housing, made of a special stainless steel in order to protect the camera in presence of corrosive elements. The shooting window is protected by a germanium glass that is transparent in the thermal wavelengths, and is equipped with a mechanical device covering the germanium glass. This cover has the dual function to allow the microbolometric sensor calibration and to preserve the integrity and the cleanness of the shooting window during the standby of the thermal camera.

The RMS directly manages the phase of the image shots by running in succession the execution of the following actions: (1) turns the thermal camera on, (2) waits for the calibration of the microbolometric sensor, (3) opens the watertight cover, (4) sets the sensibility, the range levels and focus parameters, (5) waits for the image acquisition, (6) closes the watertight cover, (7) uploads the image data acquired by the thermal camera in numerical format through serial RS 232C interface, (8) turns the thermal camera off.

The control unit is located at the surveillance centre of the Osservatorio Vesuviano - INGV in Naples . Its main feature is to manage the remote stations network (another similar station is operating at Vesuvio crater) through a communication system based on two different technological solutions: a master transmission system via GSM frequency network and an emergency system on radio frequency network. The control unit communicates with the RMS's allowing to both configure times and shooting parameters for the image acquisition and run the automatic uploading of the remotely acquired thermal images. In addition, the control unit performs the storage of the transferred thermal images both in its proprietary graphic format for data visualization and, after real-time data conversion in form of digital ASCII matrix containing the temperature values for further processing.

The scene that the station systematically acquires is shown in Figure 3a-b in the spectral range of the visible and IR. This scene includes part of the SE inner slope of the Solfatara crater where most radiant pixels correspond to the location of the major fumaroles (BG ~160°C and BN ~150°C), which are sited at the intersection of two active, SW-NE and NW-SE, main faults of CF (Fig. 2b). This area is the most active sector of the crater. On the basis of previous investigations [*Chiodini et al.,* 2001], it can be estimated that this area releases diffusively ~ 15% of the total CO_2 and heat released by Solfatara crater (i.e. ~ 250 t d^{-1} and ~ 13 MW respectively).

The TIR***[AC5]*** (Thermal IR) image framing covers a viewing distance that ranges from 40 m up to a maximum of about 500 m (Fig. 2b), with the main fumarole field located at an average distance of about 300 m. The increasing viewing distance produces an increase in the pixel size (Table 1) and consequently a decrease in the image resolution**.**

2.2 The October 2004 – January 2007 data set

The installation of the Solfatara monitoring station ended in mid-September 2004 and, after about one month of tests performed on the whole system, the systematic thermal imaging acquisition began on 17th October 2004. IR images were collected during night-time with the rate of three images per night (typical time acquisition 00:00, 02:00, 04:00 UTC).

The TIR imagery was generally of good quality, though it suffers from two minor problems related to the weather conditions: (1) the occasional presence of wide blurred areas due to the condensation of water vapor from the fumaroles plume and (2) the rare occurrence of heavy rain which caused the homogenization of the IR temperature. These images of very low quality were removed from the analyzed dataset which consist of 2175 TIR images from the 17th October 2004 up to 31st January 2007.

In order to investigate the dependence of IR temperatures on environmental parameters we used data acquired by a meteorological station located in the same site of the IR station. The meteorological station acquired, at 10-second intervals, the barometric pressure, wind speed, air temperature, air relative humidity, and rainfall. Hourly mean data were transferred at the surveillance center of the Osservatorio Vesuviano - INGV in Naples by means of the GSM communication system. The meteorological station worked almost continuously throughout the monitoring period (October 2004 – January 2007) with a few interruptions rarely exceeding one week. The data measured from the meteorological station are summarized in Table 2.

2.3 In situ calibration of the IR camera

The IR camera was calibrated in situ for assessing the reliability of the IR temperatures in a large temperature interval to evaluate the necessity to apply suitable corrections. The experiment consisted in the comparison between IR temperatures and temperatures measured with a K type thermocouple (hereafter named T_ther). The thermocouple was installed with an automatic data logger at an easily identified target (the wood wall of a cabin located in the central sector of the IR scene, Fig.3a-b) whose IR temperature was estimated as the average temperature of 4 pixels located in the center of the cabin wall (hereafter named T_target). The experiment started on the 1st of August 2006 and ended on the 3rd of January 2007 producing 434 pairs of T_ther and T_target values ranging from 273 to 301 K. The temperatures registered by the two independent methods are compared in the chronogram of Fig 4 and in the scattered plots of Fig. 5. Even though the IR measurements (T_target) resulted systematically lower than T_ther, the results are very good: the two temperatures strictly follow the same temporal pattern and show a very high correlation (R^2 = 0.989).

On the basis of these results we decided not to apply any instrumental correction to the raw data. This choice was made also because we did not consider another source of uncertainty which arises from viewing the surface at an oblique angle [*Ball and Pinkerton*, 2006], an effect which is difficult to be evaluated for every pixel of the image. The availability of a long time series of the same scene, allowed us to analyze the collected thermal imagery in terms of relative temperature variations without applying any correction for the oblique angle view whose possible effects remained unchanged at each location during the monitoring period.

3. Results

3.1 Meteorological parameters affecting IR images

Meteorological data and IR temperatures were combined in a single dataset, such that each IR image had corresponding values of the meteorological parameters. The objective was to statistically analyze the dependence of the IR temperatures with environmental parameters.

The correlation coefficients between the mean temperature of the scene excluding the sky (SES, a matrix of 320 x 190 pixel) and the meteorological parameters are listed in Table 3. The data indicate that the air temperature is by far the most important parameter related to the SES temperature (r = 0.98). Pressure and wind speed have a moderate correlation, but significant at the 95% confidence level, with SES temperature (r=-0.17 and r=-0.19, respectively) whereas air relative humidity is not significantly correlated. A multi parametric regression analysis was then applied to quantify the relation between the SES mean temperature, used as dependent variable, and the meteorological parameters considered as independent variables. The stepwise model of regression showed that the air temperature alone explains about 96% of the SES mean temperature variance, while the addition of the other two significant variables nly provides an extra 1%.

Further applications of the regression analysis regarded the mean temperature of 40 boxes (40*40 pixels) on which the IR scene was divided. The results show an high correlation of the IR temperature with air temperature in any portion of the image. In particular the air temperature explained an amount of the IR temperature variance of the 40 boxes from 92% to 97%, with a mean value of about 95%. A strict dependence of the IR temperature on air temperature was observed also in the main fumarolic area (MFA, Fig. 3) where the air temperature explained 92% of MFA mean temperature variance.

The high correlation with air temperature implies a strong seasonal control on the IR temperatures registered by the camera both for SES area as well for the MFA (Fig. 6a). In order to highlight temperature changes caused by variations in the endogenous source, this dominant effect from environmental parameters has to be removed from the data. Among different possibilities we chose T_target as reference to filter the IR data from ambient conditions because T_target was easily computable for each IR image, strictly depended on ambient temperature and refers exactly to the same meteorological conditions of each image, and finally it was not affected by variations of the endogenous source. The filtering operation consisted of subtracting from the IR temperature (T) of each pixel the T_target of the same image. The values obtained (T-T_target, Fig. 6b) do not show the typical seasonal pattern of ambient temperature which instead characterizes the measured IR temperatures (Fig. 6a). This filtering worked suitably for both IR temperatures, that were not anomalous, and IR temperatures of hot areas (Fig. 6b, SES and MFA lines).

The IR image quality (i.e. sharpness, contrast, brightness, etc.) is another feature which depends on meteorological conditions and which needs some consideration because it can strongly affect the possibility of recognizing thermal anomalies in the scene. The standard deviation (SD) of the IR temperatures can be considered as a good index of the quality of each image. During the monitoring period SD of the SES varied from ~2 to ~ 6 (Fig. 7). The highest values correspond to the sharpest images while the lowest characterize the blurred, lowest quality images as highlighted in Fig. 8a and 8b where an image with a high SD (SD = 6.24, image of the 4th April 2005, hour 4.00) is compared with an image of low SD (SD = 2.16, image of 21st April 2005, h 0.00). Fig. 7 shows how the lowest SD values generally correspond to periods of rain. Excluding data acquired during rain periods, it is evident the negative correlation between SD and H_2O concentration in air (Fig. 9) which reflects the homogenization of the temperature in the IR scene due to the increase in both the atmospheric absorption and scattering. It is worth noting that the quality of the image does not affect the T-T_target values of the entire area which are not correlated to SD (Fig. 10). Most probably this reflects the fact that the water vapor air concentration affects, in a similar extension, both the background temperatures of the image and the temperatures of the target. Instead the T-T_target values of the hot zones were strongly affected by the quality of the image as suggested by the positive correlation between SD and the MFA T-T_target values (Fig. 10). This correlation between T-T_target values of the hot zones and the SD, i.e. the quality of the image, may depend on different factors. For example, during wet periods, the presence of a bigger plume of condensed steam in the fumarolic areas can enhance air IR absorption and scattering. Moreover during rain and in the following wet periods, the actual temperature of the hot soils can decrease causing negative peaks on T-T_target values. Beside the causes of this effect, during the monitoring period, this dependence of T-T_target on the image quality in the hot zones resulted in more random scatter of T-T_target as highlighted by the noise of the MFA line in Fig. 6b.

In conclusion, the study of the correlation between IR images and meteorological parameters showed as the IR average temperatures are mainly controlled by ambient temperature while the quality of the image, here quantified in terms of SD, is inversely correlated with the water vapor concentration in air. In addition rain events produce an anomalous decrease of SD values because cause the homogenization of the surface temperatures. Contrary periods of clear, not humid air, will tend to produce more contrasted images characterized by highest SD values.

3.2 Slow movements of IR scene and image co-registration

Fig. 6b suggests that no evident temperature anomalies affected the whole monitored scene, but we can not exclude that smaller portions of the Solfatara crater were affected by temperature changes. A pixel by pixel linear regression of T-T_target with respect to time was performed in order to investigate local temperature changes of the scene. Ten-day average values of T-T_target at each pixel were considered in order both to reduce the computation time and to smooth high frequency variations. The results are graphically reported in the map of Fig. 11a.

The map, which represents the temperature change expressed as K/year, highlights a series of positive and negatives structured anomalies. At all locations a positive anomaly systematically corresponds to a negative anomaly located to the left and below by a few pixels, suggesting that a movement of the camera occurred during the monitoring period. This unexpected behavior complicates the identification of the real temperature change of the scene. In order to do a co-registration of the images, a study of the correlations among selected portions of the scene (boxes from 1 to 8 in Fig. 11a) was performed. Practically for each box the shifts in the horizontal and in the vertical axis (DX and DY respectively, expressed as number of pixels) were determined for which the best correlation with respect to a reference case (image n. 1200, 20-02-2006) was obtained. The results are reported in the DX and DY chronograms of Figs. 12a and 12b. All the boxes, located in the SE inner slope of Solfatara crater, correspond to hot spots where the contrast with the relatively cold nearby zones makes the computation more efficient and gives the best results, i.e. less noisy DX and DY curves are obtained. It is worth noting the similarity among all the curves obtained in different portions of the scene. On the basis of these correlations it was assumed that the entire IR scene moved both synchronously and at the same velocity following the mean DX and DY vs. time patterns highlighted in Figs. 12a and 12b. This homogeneous behavior of the entire scene suggests that a slow movement affected the camera.

It is reasonable to suggest that a local deformation of the terrain could have caused the tilt of the pole where the camera is installed and the consequent movement of the scene. We can not exclude that this local deformation is linked to the general terrain uplift phase which occurred at Campi Flegrei in 2005-2006 [*Troise et al.,* 2007]. The chronograms of the mean DY displacement (vertical displacement of the scene) registered by the IR camera are compared in Fig. 13a with the ground uplift registered by RITE and ACAE GPS stations located in the region of the Solfatara (Fig. 2). Because the different total displacement registered by the two stations during the period (48 mm and 36 mm at RITE and ACAE respectively), the GPS data were normalized. The DY curve is very similar to the GPS normalized data with the only difference that the DY movement precedes the ground uplift registered at RITE and ACAE. The best correlation between DY and GPS measurements is found shifting the ACAE and RITE datasets back by ~100 days (Fig. 13b). This correlation, if confirmed by the data which will be acquired in the next years, would imply that Solfatara is affected by a ground motion that precedes the ground deformation pattern generally observed at other locations in the CF.

Finally the DY and DX mean values (Fig. 12a-b) were used to perform the co-registration of all the images assuming as reference (DX=0, DY=0) the image n. 1200 (acquired on 20-02-2006). Practically for each pixel of each image a new value of T-T_target was computed as the average of the values of the 4 pixels located in the new position and weighted in function of the surface contribution.

3.3 Temperature variations at Solfatara

A pixel by pixel regression with respect to time of the corrected T-T_target data (averaged on a 10-day period) was performed and the results are graphically shown in Fig. 11b. The map does not show any more the structural alternation of positive and negative anomalies which characterized the analogue picture obtained from the uncorrected values (Fig. 11a). This suggests that in general the adopted correction was effective and that Fig. 11b can be used to investigate temperature changes that occurred at Solfatara during the monitoring period.

Temperature variations affected both the Solfatara crater wall and the areas of the plane nearest to the camera. Here we focus on the variations of the Solfatara crater wall being the variations of the plane of smaller dimension and most probably linked to very local processes. The map of Fig. 11b suggests that generally the SE inner slope of the Solfatara crater was not affected by important temperature changes, being these generally restricted in the interval from -0.5 K/year to 0.5 K/year. The map however highlights the presence of some spots characterized by higher temperature increases (red and white colors) and few spots which cooled (blue color).

Before discussing the details of the temperature variations, it is necessary to describe briefly the data filtering adopted to compare images of different quality. For example we examined the temperature increase registered by the area BG (Fig. 14), i.e. the biggest and hottest fumarole of Solfatara. In the scene this area corresponds to 18 pixels whose average T-T_target values during the monitoring period are shown in Fig. 14b. The data are highly scattered because different meteorological conditions caused different image qualities and a large variability of the SD of this image sector (SD-MFA Fig. 14a). In order to filter the temperatures from this “image quality” effect, only the data corresponding to a narrow interval of SD were considered. The images with a SD-MFA from 7.7 to 8.8 (gray band in Fig. 14a) were chosen for the zones located in the MFA (i.e. areas of BG and BN fumaroles) while for the other zones the filtering was based on SD-SES (values from 4 to 4.6). A further improving of the temperature vs. time data was obtained by averaging the data of the images of the same time period. For example Fig. 14c shows the 1 day mean of T-T_target values of BG area filtered for SD-MFA values (T_fltr).

The T_fltr vs. time curve (Fig. 14c) shows a first period (autumn 2004 – autumn 2005) of minor variations followed by a period of temperature increase with two relative peaks, a first one from November 2005 to February 2006 and the second one from November 2006 to January 2007. In total, from Nov. 2005 to Jan. 2007, the BG area heated ~ 5-10°C. This temperature increase was not, however, reflected in the maximum temperature of BG fumarole which, in the period of IR monitoring, remained at a stationary value of 161 ± 2°C. The temperature increase observed in the nearby hot soils was most probably the result of an increased flux of fumarolic fluids, while the absolute temperature of BG did not change. It is worth noting that also steam velocity, a parameter monitored since spring 2005 at BG fumarole, displayed a temporal trend very similar to the IR temperature pattern, reinforcing the idea that the anomaly is caused by an increase in the flux of the fumarolic fluids (Fig. 15).

The fact that a temperature peak similar to those observed in 2005 and 2006 was not observed in autumn 2004 seems to exclude the possibility that the two temperature increases being linked to some seasonal effect not removed by the T_target correction. To the contrary we think that the observed anomalies are caused by variations in the deep source of fluids. Both the anomalous increases of the temperature followed two periods of increased seismicity by a few days to weeks (Fig. 15). The first seismic swarm occurred on 5th October 2005 when 84 low energy volcano-tectonic (VT) events (M_{max}= 1.1) were registered, while the second period occurred from 19 to 27 October 2006 and was characterized by ~ 150 VT earthquakes (M_{max}=0.8) and more than 750 long-period (LP) events [*Saccorotti et al.*, 2007]. All the events of both periods were clustered beneath Solfatara crater; the VT events occurred at depths of 1.5-2.5 Km while the LP at shallower depths (~ 500 m, Fig. 16). These data suggest that the temperature anomaly registered at BG area was most probably caused by the transfer of hot fluids from the deeper part of the hydrothermal system to the Solfatara discharge zone. The time lag between the occurrence of the seismic shocks at depth and the temperature peaks at BG would be due to the time necessary for the fluid to move from the deeper seismogenetic zones to the surface. Similar changes in temperature after the October 2005 seismic crisis were observed in other localized spots of the fumarolic field (Fig. 17, i.e. 10-day T_fltr mean values of areas a, b, c, d, e in Fig. 11b).

Fig. 11b shows that the temperature increase, which is particularly evident at BG site, did not affect the entire fumarolic field. Instead some spots cooled (blue color in Fig. 11b) but these temperature decreases were not linked to the variation of the hydrothermal source rather they reflect anthropogenic activity or vegetation growth. In particular the BN site, another strong fumarole of high temperature (~ 150°C), was affected during 2006 by a marked cooling. In this case the temperature variation registered by the automatic station was caused by the building in October-November 2006 of a tourist pathway that goes around the BN fumarole. This work caused a clear decrease of the temperature of the area (Fig. 18a). Other temperature decreases were observed in the area labeled 'vegetation – v1' in Fig. 11b. In this case the temperature decrease, that was registered from April to June of both 2005 and 2006 (Fig. 18b) reflects the fact that the relatively hot pixels of the Solfatara crater wall were progressively occupied by the colder vegetation growing in the spring season. The same process explains also the positive anomalies at the border between the sky and the ground ('vegetation – v2' in Fig. 11b), being in this case the relatively cold pixels of the sky progressively occupied by the hotter vegetation.

4. Summary and Conclusions

The energy dissipated daily by hydrothermal hot soils generally represents a main term of the total energy released from volcanoes. At Solfatara for example the thermal energy released in the last 30 years by the hot soils is much higher not only than the conductive heat flux over the caldera (90 km^2) but even than the average energy release associated to seismic activity and ground deformation during the same period. The spatially extensive monitoring of such energy fluxes was the main objective of this research. In particular we tested the possibility to use an infrared (IR) automatic station to monitor the shallow thermal structure of hydrothermal zones. With respect to previous IR applications, most of which regarded the study of relatively quick processes associated to volcanic eruptions, our experiment was designed to detect and quantify slow temperature changes of shallow thermal structures of quiescent volcanoes over long periods. A significant portion of the Solfatara fumarolic field was monitored with the systematic acquisition of IR images from a permanent station. The system prototype was built and tested at Solfatara in autumn 2004, and has since produced 2175 thermal images of the same scene up to January 2007.

The reliability of the data was tested with an in situ calibration procedure, performed by comparing IR temperatures with those given by a K type thermocouple. The IR measurements resulted systematically lower than the thermocouple temperatures, but the two sets of data showed a very high correlation. The satisfactory result allowed us consider the data without any instrumental corrections. Meteorological data were specifically acquired during the experiment in order to investigate the dependence of IR data on environmental parameters. IR temperatures are correlated to air temperature which explained 92%-97% of the IR temperature variance. This implies a strong seasonal control on the IR temperatures of both background and hot areas of Solfatara at the surface. In order to remove the effect of ambient temperature variations, which masks the variation caused by endogenous changes, a simple background correction was applied to all the data. We investigated the quality of the images (i.e. sharpness, contrast, etc.) which was also found strongly affect the possibility to recognize temperature anomalies. For quantifying the image quality we used the standard deviation (SD) of the IR temperatures of the images. The image quality was inversely correlated with the water vapor concentration in the air. In order to study the temporal evolution of the monitored thermal structure we thus adopted a simple ‘quality image’ filter based on SD values. A further correction of the images was necessary to remove the effects of a slow movement of the camera and to obtain the corrected data set suitable to investigate the thermal variations.

Anomalous temperature increases were recorded at the area named BG, i.e. the main fumarole at Solfatara, in autumn 2005 and 2006, a few days to weeks after the occurrence of seismic swarms which were located exactly beneath Solfatara crater. This delay between the temperature anomalies and the end of the seismic swarms excludes the possibility that such temperature anomalies were co-seismic effects. In our model episodes of fluid pressure increases within the hydrothermal system caused both the seismic events and, some time later, the temperature anomalies at the surface, related to the expulsion of fluids. Similar temperature increases were observed in several spots of the scene, while all the temperature decreases were caused either by anthropogenic activity or vegetation growth.

The final considerations are devoted to the general lesson which we learned at Solfatara analyzing for the first time a two-years long series of IR images.

The system gives a reliable picture, rich in datails, of the temperature changes and important indications on the origin of the changes. It is worth noting that these signs were detected in a system currently characterized by a level of activity relatively low with respect to those systems affected by real volcanic crisis where more spectacular results would be expected.

Finally, an important point is that the images can be suitably filtered from ambient effects using simple corrections based on data contained in the image itself. This makes the system independent from the availability of other data. Our filtering was based in fact on a background temperature defined in the scene, on the standard deviation of each image and on a procedure based on image data for the co-registration. These features make the system almost autonomous and able to work also in remote and impervious sites resulting as a suitable tool for volcanic surveillance.

5. Acknowledgments

We would like to thank the Associate Editor and the reviewers Cynthia Werner and Salvatore Inguaggiato for their positive comments and useful suggestions that helped to improve the paper. We thank Prospero De Martino and Umberto Tammaro for the GPS data. We are grateful to Antonio Costa for the constructive comments on the manuscript. The TIIMNet project was partially founded by the National Operating Program. This work was partially funded by the Italian Dipartimento della Protezione Civile in the frame of the 2004–2006 agreement with Istituto Nazionale di Geofisica e Vulcanologia – INGV and by European Project VOLUME.

6. References

Bailey, J. E., A. J. L. Harris, J. Dehn, S. Calvari, and S. Rowland (2006), The changing morphology of an open lava channel on Mt. Etna, *Bull. Volcanol.*, *68*, 497- 515.

Ball, M., and H. Pinkerton (2006), Factors affecting the accuracy of thermal imaging cameras in volcanology, *J. Geophys. Res.*, *111*, B11203.doi:10.1029/2005JB003829.

Barberi, F., G. Corrado, F. Innocenti, and G. Luongo (1984), Phlegrean Fields 1982– 1984: Brief chronicle of a volcano emergency in a densely populated area, *Bull. Volcanol.*, *47*, 175- 185.

Battaglia, M., C. Troise, F. Obrizzo, F. Pingue, and G. De Natale (2006), Evidence for fluid migration as the source of deformation at Campi Flegrei Caldera (Italy), *Geophys. Res. Lett.*, *33*, L01307.doi:10.1029/2005GL024904.

Caliro, S., G. Chiodini, G. Galluzzo, G. Granieri, M. La Rocca, G. Saccorotti, and G. Ventura (2004), Recent activity of Nisyros volcano (Greece) inferred from structural, geochemical and seismological data, *Bull. Volcanol.*, *67*, 358–369.doi:10.1007/s00445-004-0381-7.

Calvari, S., and H. Pinkerton (2004), Birth, growth and morphologic evolution of the 'Laghetto' cinder cone during the 2001 Etna eruption, *J. Volcanol. Geotherm. Res.*, *132*, 225-239.

Calvari, S., L. Spampinato, L. Lodato, A. J. L. Harris, M. R. Patrick, J. Dehn, M. R. Burton, and D. Andronico (2005), Chronology and complex volcanic processes during the 2002 - 2003 flank eruption at Stromboli volcano (Italy) reconstructed from direct observations and surveys with a handheld thermal camera, *J. Geophys. Res.*, *110*, B02201.doi:10.1029/2004JB003129.

Chiodini, G., F. Frondini, C. Cardellini, D. Granieri, L. Marini, and G. Ventura (2001), CO_2 degassing and energy release at Solfatara Volcano, Campi Flegrei, Italy, *J. Geophys. Res.*, *106*, 16,213-216,221.

Chiodini, G., D. Granieri, R. Avino, S. Caliro, A. Costa, and C. Werner (2005), Carbon dioxide diffuse degassing and estimation of heat release from volcanic and hydrothermal systems, *J. Geophys. Res.*, *110*, B08204.doi:10.1029/2004JB003542, 2005.

Chiodini, G., M. Todesco, S. Caliro, C. Del Gaudio, G. Macedonio, and M. Russo (2003), Magma degassing as a trigger of bradyseismic events; the case of Phlegrean Fields (Italy), *Geophys. Res. Lett.*, *30*, 1434.doi:10.1029/2002GL016790.

Dean, K. G., J. Dehn, K. R. Papp, S. Smith, P. Izbekov, R. Peterson, C. Kearney, and A. Steffke (2004), Integrated satellite observations of the 2001 eruption of Mt. Cleveland, Alaska, *J. Volcanol. Geotherm. Res.*, *135*, 51- 73.

Di Vito, M. A., R. Isaia, G. Orsi, J. Southon, S. De Vita, M. D'Antonio, L. Pappalardo, and M. Piochi (1999), Volcanism and deformation since 12,000 years at the Campi Flegrei caldera (Italy), *J. Volcanol. Geotherm. Res.*, *91*, 221-246.

Harris, A. J. L., J. Dehn, M. R. Patrick, S. Calvari, M. Ripepe, and L. Lodato (2005), Lava effusion rates from hand-held thermal infrared imagery: an example from the June 2003 effusive activity at Stromboli, *Bull. Volcanol.*, *68*, 107-117.

Harris, A. J. L., L. P. Flynn, O. Matias, W. I. Rose, and J. Cornejo (2004), The evolution of an active silicic lava flow field: An ETM+ perspective, *J. Volcanol. Geotherm. Res.*, *135*, 147-168.

Harris, A. J. L., and A. J. H. Maciejewski (2000), Thermal surveys of the Vulcano Fossa fumarole field 1994- 1999: Evidence for fumarole migration and sealing, *J. Volcanol. Geotherm. Res.*, *102*, 119- 147.

Hellman, M. J., and M. S. Ramsey (2004), Analysis of hot springs and associated deposits in Yellowstone National Park using ASTER and AVIRIS remote sensing, *J. Volcanol. Geotherm. Res.*, *135*, 195- 219.

Hochstein, M. P., and C. J. Bromley (2005), Measurement of heat flux from steaming ground, *Geothermics*, *34*, 133-160.

Ingebritsen, S. E., D. L. Galloway, E. M. Colvard, M. L. Sorey, and R. H. Mariner (2001), Time-variation of hydrothermal discharge at selected sites in the Western United States: Implications for monitoring, *J. Volcanol. Geotherm. Res.*, *111 (1-4)*, 1-23.

Johnson, J. B., A. J. L. Harris, and R. P. Hoblitt (2005), Thermal observations of gas pistoning at Kilauea Volcano, *J. Geophys. Res.*, *110*, B11201.doi:10.1029/2005JB003944.

Kaneko, T., and M. J. Wooster (1999), Landsat infrared analysis of fumarole activity at Unzen Volcano: time-series comparison with gas and magma fluxes, *J. Volcanol. Geotherm. Res.*, *89*, 57-64.

Lautze, N. C., A. J. L. Harris, J. E. Bailey, M. Ripepe, S. Calvari, J. Dehn, S. K. Rowland, and K. Evans-Jones (2004), Pulsed lava effusion at Mount Etna during 2001, *J. Volcanol. Geotherm. Res.*, *137*, 231- 246.

Lodato, L., L. Spampinato, A. J. L. Harris, S. Calvari, J. Dehn, and M. Patrick (2006), The morphology and evolution of the Stromboli 2002-2003 lava flow field: an example of a basaltic flow field emplaced on a steep slope., *Bull. Volcanol.*doi: 10.1007/s00445-006-0101-6.

Oppenheimer, C., P. W. Francis, D. A. Rothery, R. W. T. Carlton, and L. S. Glaze (1993), Infrared image analysis of volcanic thermal features; Lascar Volcano, Chile, 1984-1992, *J. Geophys. Res.*, *98*, 4269-4286.

Oppenheimer, C., and G. Yirgu (2002), Thermal imaging of an active lava lake; Erta ’Ale Volcano, Ethiopia, *Int. J. Remote Sens.*, *23*, 4777-4782.

Pinkerton, H., M. James, and A. Jones (2002), Surface temperature measurements of active lava flows on Kilauea volcano, Hawai’i., *J. Volcanol. Geotherm. Res.*, *113*, 159-176.

Ramsey, M. S., and J. H. Fink (1999), Estimating silicic lava vesicularity with thermal remote sensing; a new technique for volcanic mapping and monitoring, *Bull. Volcanol.*, *61*, 32-39.

Saccorotti, G., S. Petrosino, F. Bianco, M. Castellano, D. Galluzzo, M. La Rocca, E. Del Pezzo, L. Zaccarelli, and P. Cusano (2007), Seismicity associated with the 2004-2006 renewed ground uplift at Campi Flegrei caldera, Italy., *Submitted to Physics Earth Planet. Inter.*

Sorey, M. L., B. M. Kennedy, W. C. Evans, C. D. Farrar, and G. A. Suemnicht (1993), Helium isotope and gas discharge variations associated with crustal unrest in Long Valley Caldera, California, 1989-1992, *J. Geophys. Res.*, *98*, 15,871-15,889.

Todesco, M., and G. Berrino (2005), Modeling hydrothermal fluid circulation and gravity signals at the Phlegraean Fields caldera, *Earth Planet. Sci. Lett.*, *240*, 328-338.

Todesco, M., J. Rutqvist, G. Chiodini, K. Pruess, and C. M. Oldenburg (2004), Modeling of recent volcanic episodes at Phlegrean Fields (Italy); geochemical variations and ground deformation, *Geothermics*, *33*, 531-547.

Troise, C., G. De Natale, F. Pingue, F. Obrizzo, P. De Martino, U. Tammaro, and E. Boschi (2007), Renewed ground uplift at Campi Flegrei caldera (Italy): New insight on magmatic processes and forecast., *Geophys. Res. Lett.*, *34*, L03301.doi:10.1029/2006GL028545.

Vaughan, R. G., S. J. Hook, M. S. Ramsey, V. J. Realmuto, and D. J. Schneider (2005), Monitoring eruptive activity at Mount St. Helens with TIR image data, *Geophys. Res. Lett.*, *32*, L19305.doi:10.1029/2005GL024112.

Watson, I. M., V. J. Realmuto, W. I. Rose, A. J. Prata, G. J. S. Bluth, Y. Gu, C. E. Bader, and T. Yu (2004), Thermal infrared remote sensing of volcanic emissions using the moderate resolution imaging spectroradiometer, *J. Volcanol. Geotherm. Res.*, *135*, 75-89.

Werner, C., S. L. Brantley, and K. Boomer (2000), CO_2 emissions related to the Yellowstone volcanic system 2. Statistical sampling, total degassing, and transport mechanisms, *J. Geophys. Res.*, *105 (B5)*, 10831-10846.

Werner, C., G. Chiodini, D. Granieri, S. Caliro, R. Avino, and M. Russo (2006), Eddy covariance measurements of geothermal heat flux at Solfatara Volcano, Naples, Italy., *Earth Planet. Sci. Lett.*, *244/1-2*, 72-82.

FIGURE CAPTIONS

Figure 1 – General view of the Solfatara crater in the spectral range of the visible and IR (range 8-14 µm). The town of Pozzuoli is in the background.

Figure 2 – a) Solfatara thermal monitoring station. b) Digital color orthophoto (CGR it2000) of the Solfatara crater area. Red lines represent faults and fractures [*Di Vito et al*, 1999]; yellow lines shows the TIR image framing. The Solfatara crater rim and the locations of the permanent GPS stations (RITE and ACAE) are also shown. BN (Bocca Nuova) and BG (Bocca Grande) are the hottest fumaroles of the Solfatara crater.

Figure 3 – Scene (320x240 pixel) acquired by the remote station a) in the spectral range of the visible and b) in the IR wavelength. The target is the wall of a wood cabin (4 pixels) located about at the same viewing distance of the main fumarolic area (MFA). BG area is also shown.

Figure 4 – Chronograms of the temperature recorded by a K type thermocouple on the wall of the wood cabin (T_ther) and temperature of the same area derived by the IR image (T_target).

Figure 5 – Thermocouple (T_ther) vs IR temperature (T_target) scatterplot.

Figure 6 – a) IR temperature variations of the whole Scene Excluding the Sky (SES, a matrix of 320x190 pixel) and of the Main Fumarolic Area (MFA, a matrix of 42 x 28 pixel) during the period October 2004 – January 2007 b) Chronograms of the same temporal series after the subtraction of the target temperature (T-T_target).

Figure 7 – Standard deviation (SD) of the SES. Rainy periods produce images with lower SD values.

Figure 8 – IR images of the scene. a) sharp image characterized by a high value of SD (SD = 6.24, image of the 4th April 2005, hour 4.00) b) blurred image with a low SD (SD = 2.16, image of 21th April 2005, h 0.00). SD is assumed as a quality index of the image.

Figure 9 – Correlation between the SD of the SES and absolute H_2O content in air (excluding rainy days).

Figure 10 – T-T_target of SES and MFA vs SD-SES. In the first case the temperature difference is not correlated to the SD, in the second one the correlation is positive.

Figure 11 – a) Map of the IR 10-day averaged temperature changes expressed in K/year. A series of contiguous positive and negative anomalies are evident. Eight boxes in the SE inner slope of Solfatara crater are selected to co register the image b) Co registration of the image with the identification of the true temperature changes. Alternations of positive and negative anomalies are disappeared and a few cooling spots (BN area) and heating spots (areas from a to e and BG area) are turned out.

Figure 12 – a) horizontal shift (DX, expressed in number of pixels) of the eight boxes (see Fig. 11) respect to a reference case (image n. 1200, 20-02-2006) and b) vertical shift (DY, expressed in number of pixels) of the same boxes. Mean DX and mean DY values are assumed as the horizontal and the vertical displacement of the whole IR scene respect to the reference case.

Figure 13 – a) Chronogram of the mean vertical displacement of the scene (mean DY, see Fig. 12) compared to the ground vertical movement recorded by the RITE and ACAE GPS stations (normalised values). b) The best correlation between DY and GPS meaurements is obtained by back-shifting ACAE and RITE data of ~100 days.

Figure 14 – a) Standard Deviation (SD) of the MFA; b) Chronogram of T-T_target rough values of the BG area; c) Chronogram of BG T-T_target values of the images characterized by SD comprises between 7.7 to 8.8 units (T_fltr). The values of the same day have been averaged. The horizontal rows mark the periods characterized by temperature increases in the BG area (Nov. 2005 – Feb. 2006 the first one and Nov. 2006 – Jan. 2007 the second one).

Figure 15 – T_fltr values of BG area, averaged over a 1-day period, are compared with the steam velocity of BG fumarole (solid dots) measured since May 2005 with a Pitot tube using the method described in the work of *Sorey et al.* [1993]. The values are normalized. The data

are compared with the number of the volcano-tectonics (VT) earthquakes located at Solfatara. In addition the arrow indicates the occurrence of 750 long-period (LP) events.

Figure 16 – Hypocentral location of the best located LP events of October 2006 [*redraw from Saccorotti et al.*, 2007]. The figure shows for comparison the position of the BG area where the thermal anomalies were detected.

Figure 17 – Chronogram of T- T_target data (averaged over a 10-day period) of 6 heating spots located in the SE inner slope of Solfatara crater (Fig. 11b).

Figure 18 – Example of chronograms of T- T_target of the cooling spots located in the SE inner slope of Solfatara crater (Fig. 11b). a) the cooling in the BN area is due to the building of a tourist pathway in October-November 2006; b) in some spots (‘vegetation–v1’ in Fig. 11b) were observed two periods of decreasing temperature (spring 2005 and 2006) in agreement with the vegetation growing.

Table 1 - Pixel surface vs. viewing distance

Distance (m)	10	30	100	300	500
Pixel size (m^2)	0.000256	0.002304	0.0256	0.2304	0.64

Table 2 - Summary of results from meteorological station of Solfatara

	Year	Mean	Range	Std.Dev.
PAtm* (hPa)	2005	998.6	971.4 : 1019.1	6.4
	2006	997.9	977.9 : 1019.7	6.0
WindS* (m/s)	2005	2.0	0.0 : 8.3	1.0
	2006	1.3	0.0 : 5.5	0.6
AirT * (°C)	2005	16.6	-0.5 : 31.3	7.1
	2006	15.7	0.7 : 30.4	6.3
AirRH* (%)	2005	74.6	33.1 : 100.0	14.2
	2006	77.9	32.9 : 100.0	14.7
	Year	Tot (mm)	Rainy_days (n)	
Rain*	2005	808.4	100	
	2006	744.0	95	

*Atmospheric pressure (PAtm in hPa), wind speed (WindS in m/s), air temperature (AirT in °C), air relative humidity (AirRH, in percentage), rainfall (Rain in mm)

Table 3 - Correlation of IR average temperature of the scene (SES, Scene Excluding the Sky) with meteorological parameters.

	PAtm(hPa)	WindS (m/s)	AirT (°C)	AirRH (%)
SES mean T (K)	-0.17	-0.19	0.98	0.00

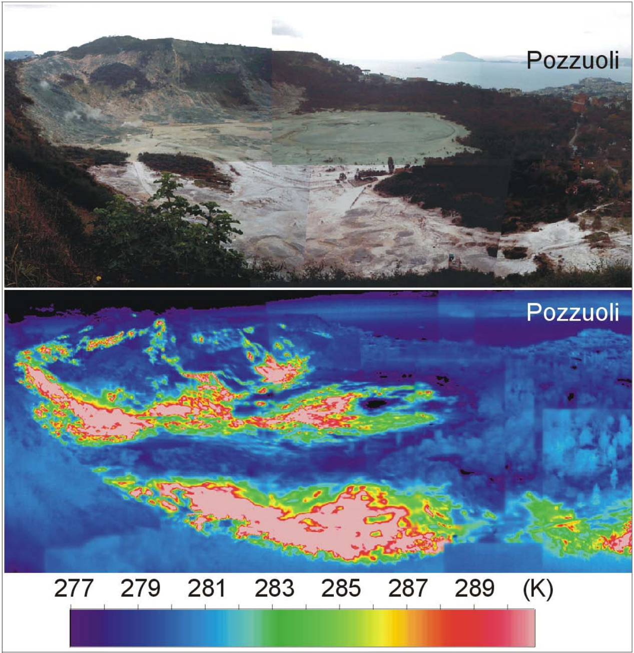
Pozzuoli
Pozzuoli
277
279
281
283
285
287
289
(K)

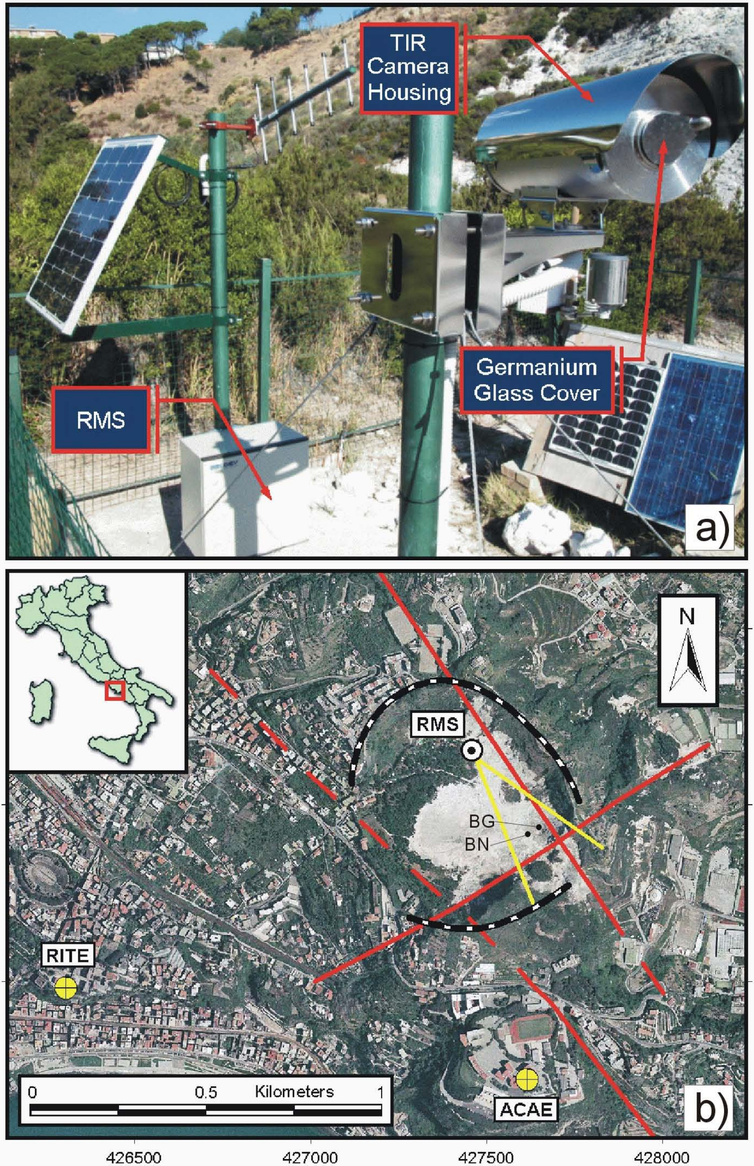
TIR
Camera
Housing
RMS
Germanium
Glass Cover
a)
N
RMS
BG
BN
RITE
ACAE
0
0.5
Kilometers
1
b)
4520500
4520000
4519500
426500
427000
427500
428000

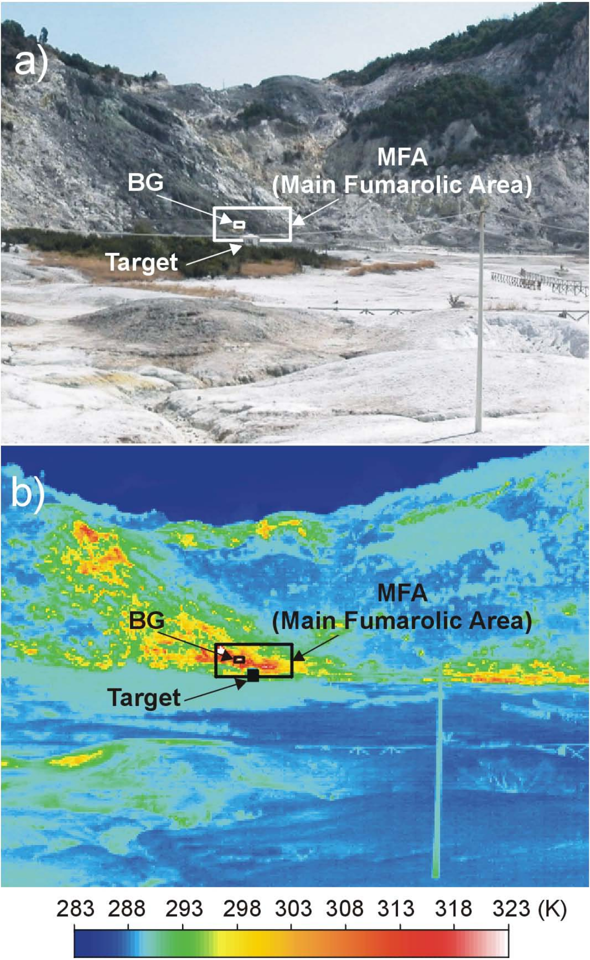

a)
MFA
(Main Fumarolic Area)
BG
Target
b)
MFA
(Main Fumarolic Area)
BG
Target
283 288 293 298 303 308 313 318 323 (K)

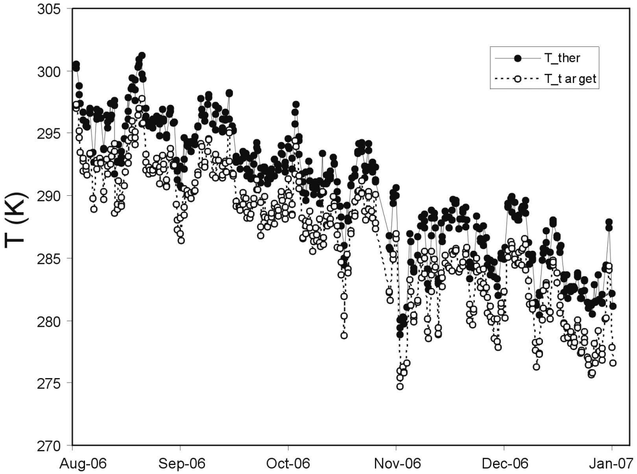
T_ther
T_t ar get
T (K)
305
300
295
290
285
280
275
270
Aug-06
Sep-06
Oct-06
Nov-06
Dec-06
Jan-07

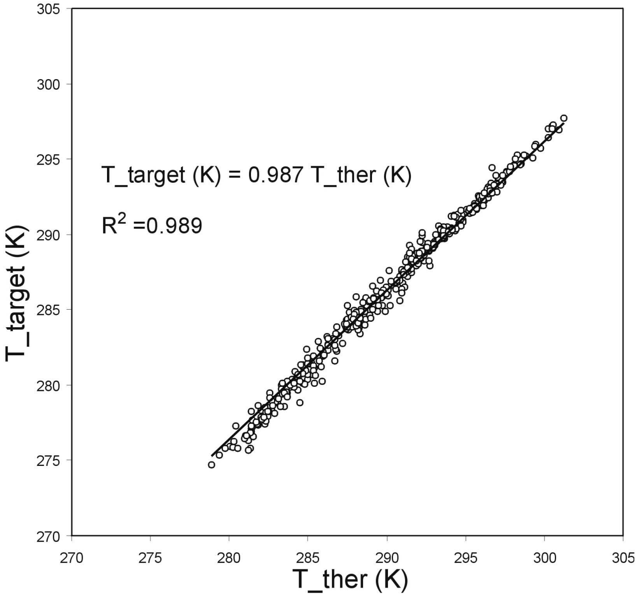

T_target (K) = 0.987 T_ther (K)
R2 =0.989
T_target (K)
T_ther (K)
305
300
295
290
285
280
275
270
270
275
280
285
290
295
300
305

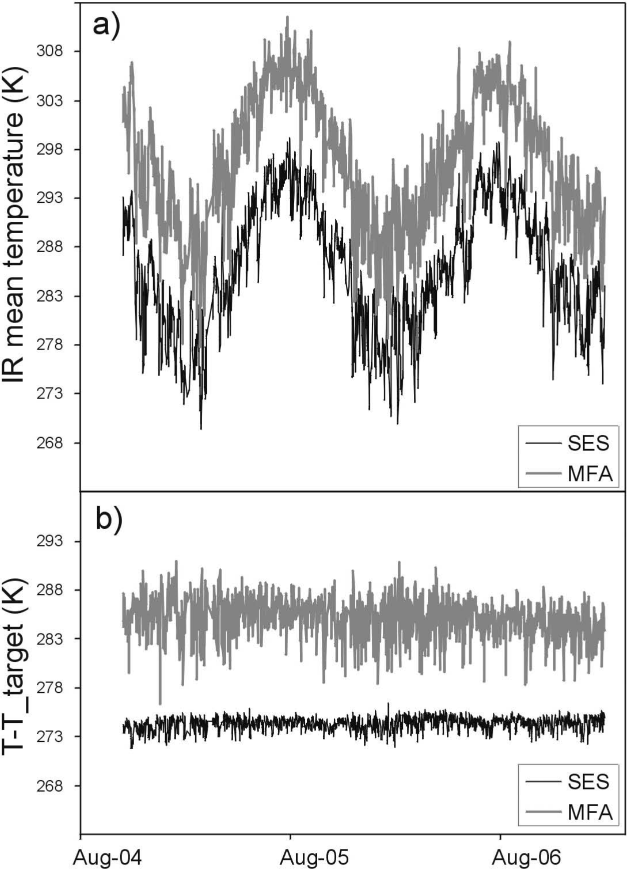
a)
IR mean temperature (K)
308
303
298
293
288
283
278
273
268
SES
MFA
b)
T-T_target (K)
293
288
283
278
273
268
SES
MFA
Aug-04
Aug-05
Aug-06

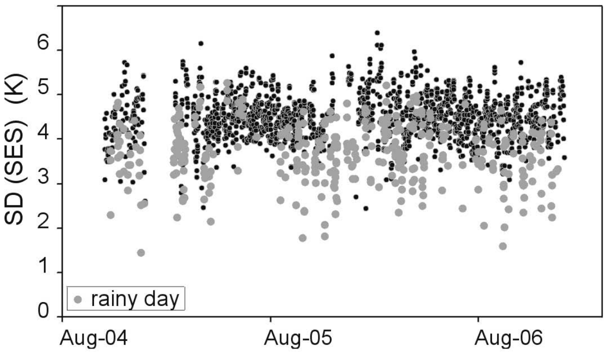

SD (SES) (K)
0
1
2
3
4
5
6
rainy day
Aug-04
Aug-05
Aug-06

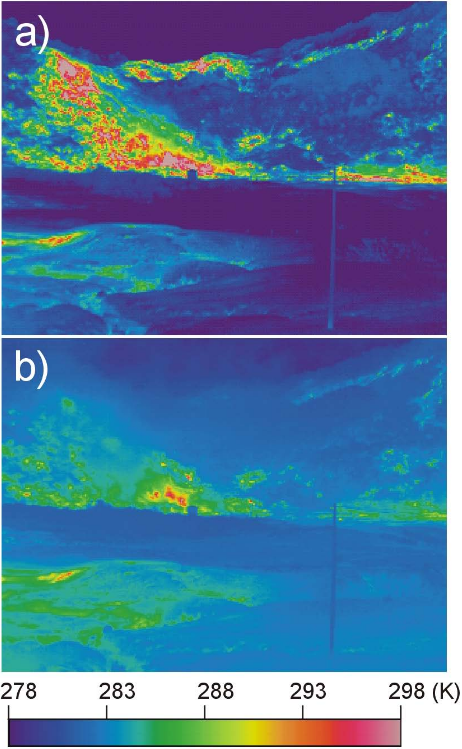
a)
b)
278
283
288
293
298 (K)

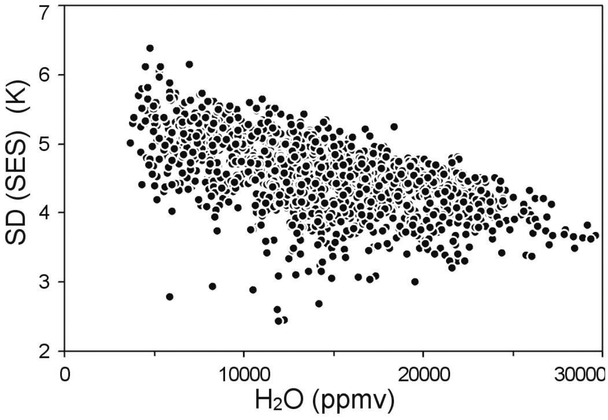
7
6
5
4
3
2
SD (SES) (K)
0
10000
20000
30000
H2O (ppmv)

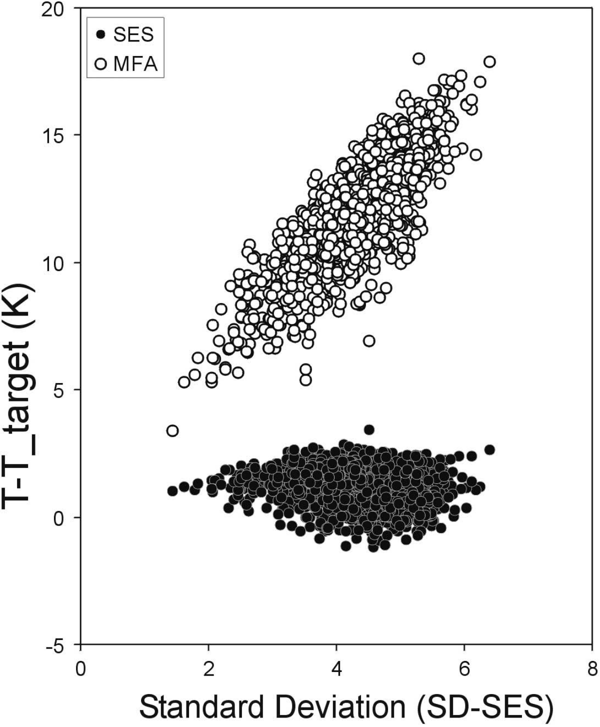
SES
MFA
T-T_target (K)
Standard Deviation (SD-SES)
20
15
10
5
0
-5
0
2
4
6
8

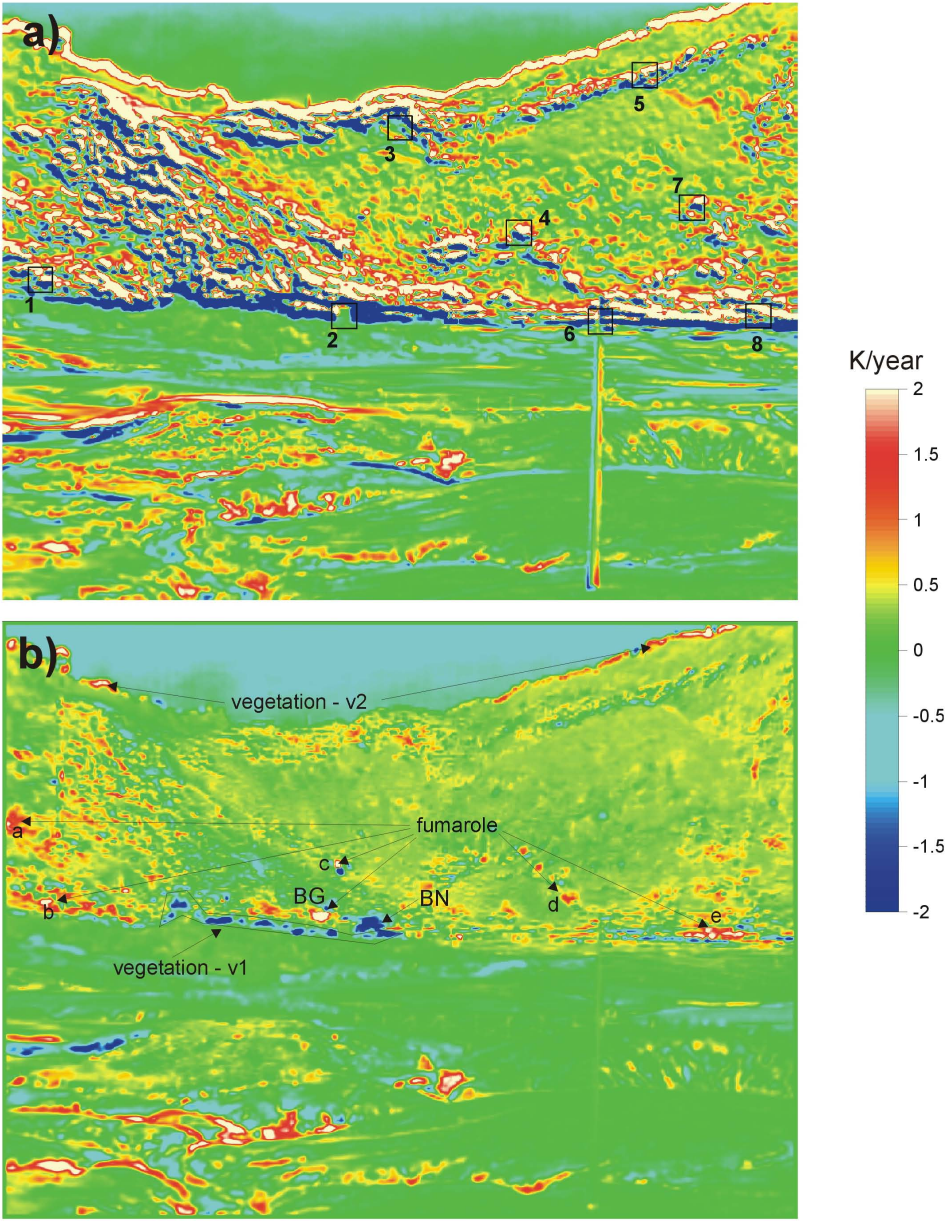
a)
1
2
3
4
5
6
7
8
b)
vegetation - v2
fumarole
a
b
c
BG
BN
d
e
vegetation - v1
K/year
2
1.5
1
0.5
0
-0.5
-1
-1.5
-2

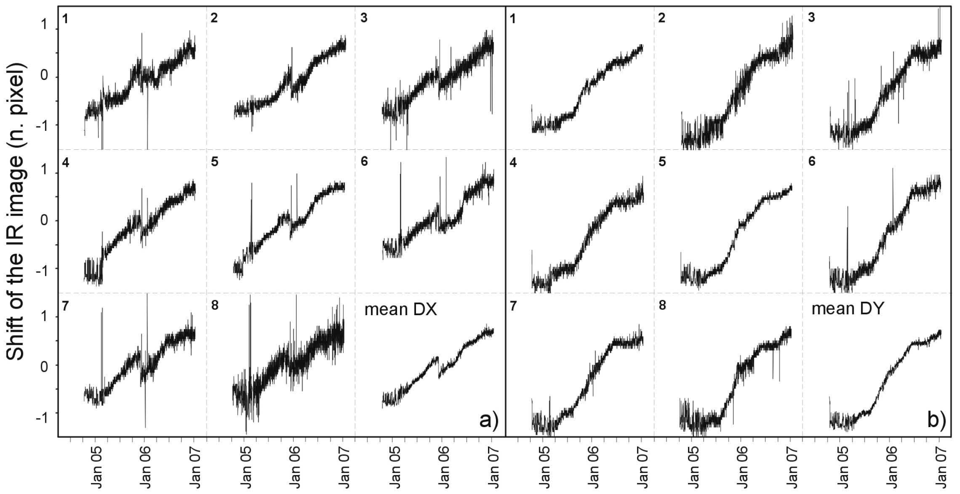

Shift of the IR image (n. pixel)
1
2
3
4
5
6
7
8
mean DX
mean DY
a)
b)
1
0
-1
Jan 05
Jan 06
Jan 07

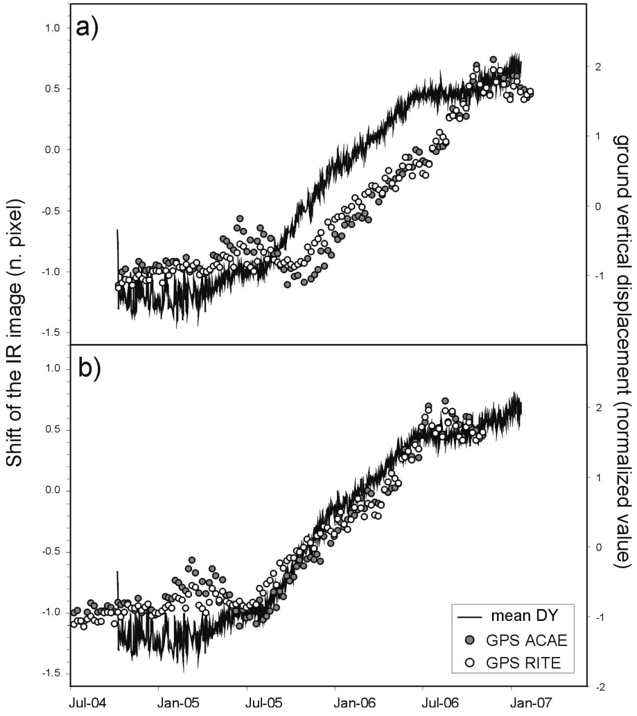

a)
b)
Shift of the IR image (n. pixel)
ground vertical displacement (normalized value)
1.0
0.5
0.0
-0.5
-1.0
-1.5
2
1
0
-1
-2
mean DY
GPS ACAE
GPS RITE
Jul-04
Jan-05
Jul-05
Jan-06
Jul-06
Jan-07

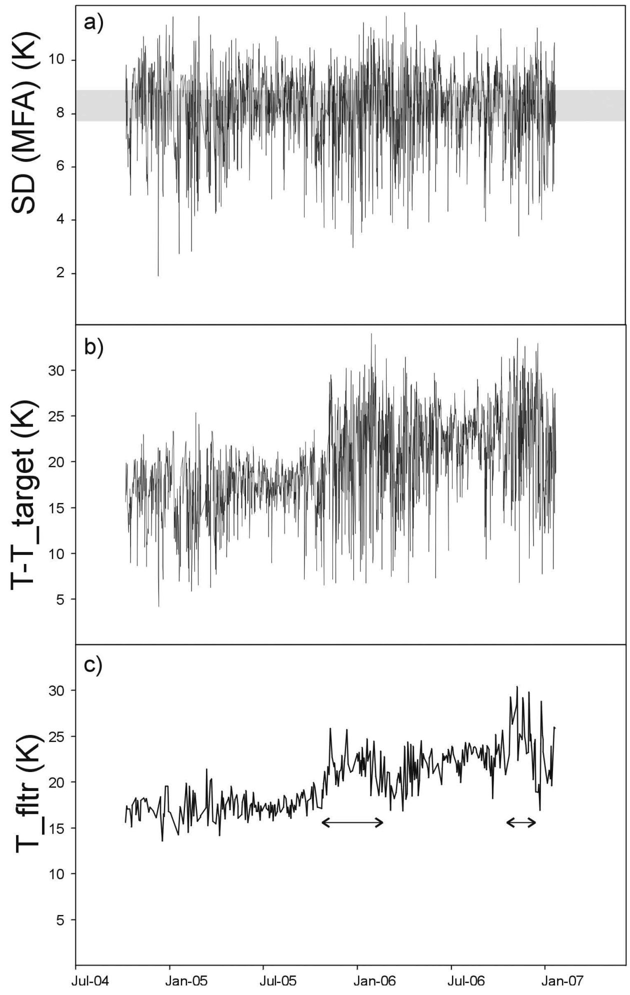

a)
SD (MFA) (K)
2
4
6
8
10
b)
T-T_target (K)
5
10
15
20
25
30
c)
T_fltr (K)
5
10
15
20
25
30
Jul-04
Jan-05
Jul-05
Jan-06
Jul-06
Jan-07

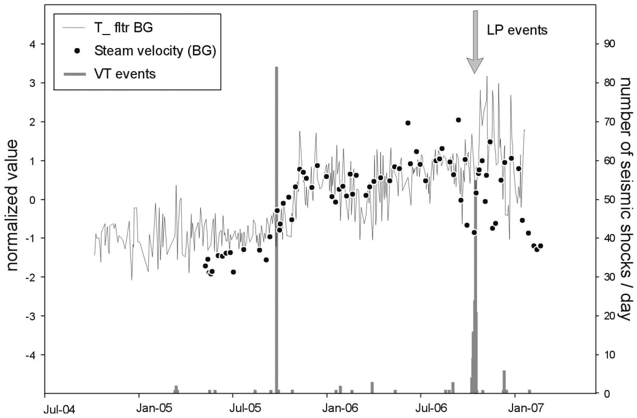
T_ fltr BG
Steam velocity (BG)
VT events
LP events
normalized value
number of seismic shocks / day
4
3
2
1
0
-1
-2
-3
-4
90
80
70
60
50
40
30
20
10
0
Jul-04
Jan-05
Jul-05
Jan-06
Jul-06
Jan-07

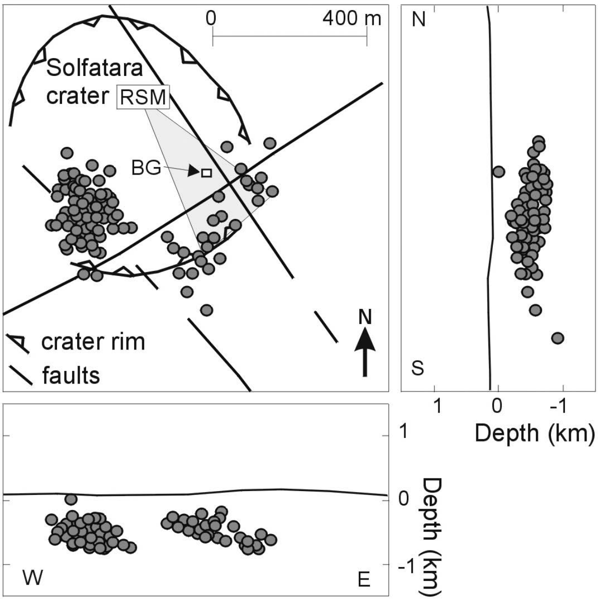
0
400 m
Solfatara
crater
RSM
BG
N
crater rim
faults
N
S
1
0
-1
Depth (km)
1
0
-1
Depth (km)
W
E

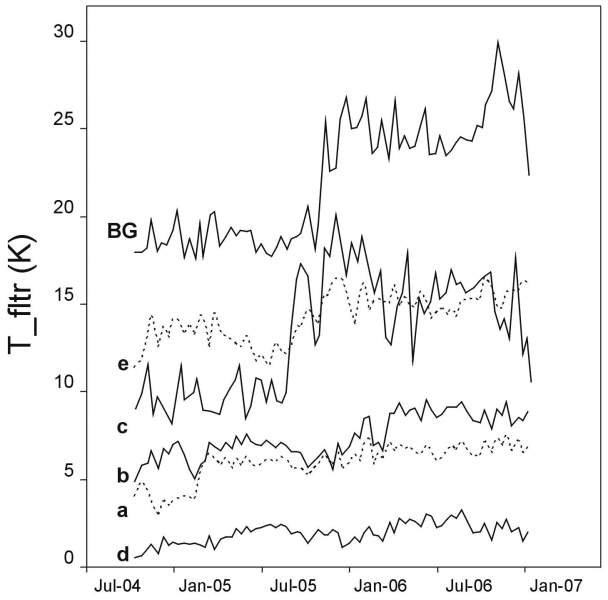
T_fltr (K)
30
25
20
15
10
5
0
BG
e
c
b
a
d
Jul-04
Jan-05
Jul-05
Jan-06
Jul-06
Jan-07

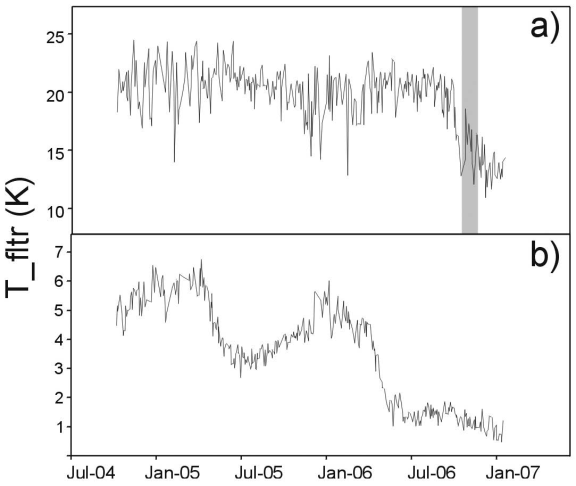

a)
b)
T_fltr (K)
25
20
15
10
7
6
5
4
3
2
1
Jul-04
Jan-05
Jul-05
Jan-06
Jul-06
Jan-07